Amplifying the Red-Emission of Upconverting Nanoparticles for Biocompatible Clinically Used Prodrug-Induced Photodynamic Therapy

Amol Punjabi,[†,±] Xiang Wu,[†,∥,±] Amira Tokatli-Apollon,[†] Mahmoud El-Rifai,[†] Hyungseok Lee,[†] Yuanwei Zhang,[†] Chao Wang,[‡] Zhuang Liu,[‡] Emory M. Chan,[§] Chunying Duan,[∥] and Gang Han*[,†]

[†]Department of Biochemistry and Molecular Pharmacology, University of Massachusetts Medical School, Worcester, Massachusetts 01605, United States, [∥]State Key Laboratory of Fine Chemicals, Dalian University of Technology, Dalian, Liaoning 116012, People's Republic of China, [‡]Jiangsu Key Laboratory for Carbon-Based Functional Materials & Devices, Institute of Functional Nano & Soft Materials (FUNSOM), Soochow University, Suzhou, Jiangsu 215123, People's Republic of China, and [§]The Molecular Foundry, Lawrence Berkeley National Laboratory, Berkeley, California 94720, United States. [±]Equal contributions.

ABSTRACT A class of biocompatible upconverting nanoparticles (UCNPs) with largely amplified red-emissions was developed. The optimal UCNP shows a high absolute upconversion quantum yield of 3.2% in red-emission, which is 15-fold stronger than the known optimal β-phase core/shell UCNPs. When conjugated to aminolevulinic acid, a clinically used photodynamic therapy (PDT) prodrug, significant PDT effect in tumor was demonstrated in a deep-tissue (>1.2 cm) setting *in vivo* at a biocompatible laser power density. Furthermore, we show that our UCNP—PDT system with NIR irradiation outperforms clinically used red light irradiation in a deep tumor setting *in vivo*. This study marks a major step forward in photodynamic therapy utilizing UCNPs to effectively access deep-set tumors. It also provides an opportunity for the wide application of upconverting red radiation in photonics and biophotonics.

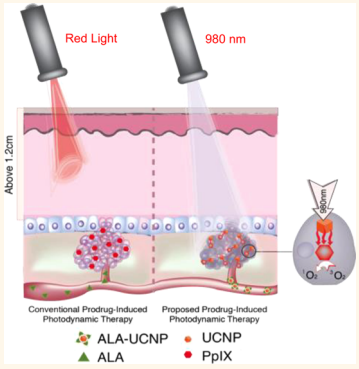

KEYWORDS: upconverting · nanoparticles · red-emission · prodrug · photodynamic therapy

Photodynamic therapy (PDT) is a favorable cancer treatment modality due to its minimally invasive nature, leading to fewer side effects than chemotherapy and less damage to marginal tissue. Treatment methods involve directly activating a photosensitizer with light irradiation in the visible region to generate singlet oxygen that is toxic to cancer cells.[1−4] Of the colors in this spectrum, longer wavelength red light (*i.e.*, 620−-670nm) is preferred by the majority of photosensitizers in clinical practice due to its improved tissue penetration.[4] Despite this advantage, efficient photodynamic therapy remains challenging in tumors at a deep tissue level (*i.e.*, >1 cm).

The current choice of FDA-approved and clinically used PDT drugs is extremely limited because only two drugs and their derivatives exist: Photofrin, a mixture of hematoporphyrin derivatives, and Levulan (5-aminolevulinic acid). Photosensitizers such as chlorin e6 and zinc phthalocyanine, although they are in clinical trials, still are experiencing complications and thus have not reached clinical practice.[5,6] Therefore, in order to accelerate advancement in PDT research, we focus on clinically used PDT drugs in this study. In contrast to the directly administered FDA-approved photosensitizer Photofrin,[3] low cost 5-aminolevulinic acid (ALA) has unique advantages as an FDA-approved PDT prodrug due to its hydrophilicity, higher selectivity in cancerous cells, and reduced concomitant photosensitivity, leading to minimal trauma in surrounding tissue.[7−10] ALA converts to the photosensitizer protoporphyrin IX (PpIX) *via* the heme biosynthesis pathway to a greater extent in tumors than in

* Address correspondence to gang.han@umassmed.edu.

Received for review July 26, 2014 and accepted September 25, 2014.

Published online September 25, 2014
10.1021/nn505051d

nonmalignant cells due to the downregulation of the enzyme ferrochelatase (a PpIX degrading factor) in cancerous cells.[11] Subsequently, under irradiation with visible light, PpIX converts triplet oxygen into singlet oxygen, inducing cell death. Despite much progress in its clinical use, ALA's application is limited because while red light offers the maximum tissue penetration of the wavelengths in PpIX's activation spectrum (Supporting Information Figure S12),[12] it is still absorbed or dispersed by pervasive components of animal tissue, rendering deep-tissue PDT quite challenging.[13−15]

With the advent of nanotechnology, lanthanide-doped upconverting nanoparticles (Ln-doped UCNP) have been developed that are excited by tissue-penetrable NIR light (*e.g.*, 980 nm) and have emissions in the visible spectrum.[16−19] We and other colleagues have reported that UCNPs can be used as transducers for PDT *in vivo*,[20,21] but despite such progress, two urgent needs have not been met: first, only model photosensitizer molecules (*e.g.*, chlorin e6, zinc phthalocyanine, *etc.*) have been explored *in vivo*; second, to the best of our knowledge, there is no conclusive evidence showing that UCNP−PDT systems induce cell death in tumors at a significant deep tissue setting beyond 1 cm deep.

To meet this first need, herein, we aimed to design and test a UCNP covalently conjugated to ALA, a clinically used PDT prodrug. To meet this second need, we anticipated that a high UCNP luminescence efficiency would enable it to induce effective deep tumor toxicity. Therefore, we intended to design a UCNP with optimal red luminescence efficiency since red light is used for PpIX (ALA's product photosensitizer) activation in clinical practice. In addition, it is important to note that, since photons in the red region penetrate tissue better than green/blue radiation, such optimal red emission UCNPs would be desirable in growing dense tumor masses where activation of the released photosensitizer molecules are distant from the UCNPs. In attempting to do so, we first revisited the current red-emitting UCNP designs. For example, hexagonal phase core/shell UCNPs with core doping concentrations of 20−30% Yb and 2% Er are arguably optimal for red-emissions, and several groups have demonstrated their potential for PDT.[21−27] To harness more upconverting efficiency for red-emissions, a couple of alternative strategies have been applied. Zhao and co-workers doped α-$NaYF_4$:Yb(20%),Er(2%) UCNPs with Mn^{2+} for enhanced emissions at 650−670 nm and loaded a variety of photosensitizers for *in vitro* PDT.[28] However, Mn-doped UCNPs offer just a 15-fold increase from weakly emitting cubic phase α-$NaYF_4$:Yb,Er UCNPs' red-emission.[29] More recently, scandium has been investigated as a host lattice material for red-emitting UCNPs: Huang and co-workers developed hexagonal phase NaScF4:Yb(20%),Er(2%) that can increase red/green emission ratio;[30] Ding *et al.* developed KScF4:Yb(20%),Er(2%) nanorods with 4.8 times the red-emission of $NaYF_4$:Yb(20%), Er(2%) nanorods.[31]

However, to the best of our knowledge, although red color purity has been achieved using the aforementioned approaches, the key problem regarding PDT remains because there is no evidence to show the red-emission of any existing UCNPs exceed that of β-$NaYF_4$:Yb(20%−30%),Er(2%)@β-$NaYF_4$, the supposed optimal red-emitting UCNP structure.[32,33] Moreover, these uncoated nanocrystals are suggested to cause ion leakage, leading to dangerous biological toxicity if applied to PDT.[34] As a result, there is an emerging demand to engineer UCNPs with enhanced NIR-to-Red outcome and better biocompatibility with respect to effective phototherapy in a deep-tissue environment.

Recently, CaF_2 has garnered attention as a shell material for Ln-doped UCNPs due to its optical transparency, stability, and small lattice mismatching with $NaYF_4$. Moreover, being a component of ossified tissues, CaF_2 shells are expected to prevent ion leakage and be more biocompatible than the conventional $NaYF_4$ shell structure.[34,35] For example, a $NaGdF_4$:Yb(20%),Er@CaF_2 was developed by Yan *et al.* for an *in vitro* PDT experiments.[36] In addition, recently, we demonstrated that the UV-emissions of α-$NaYF_4$:Yb,Tm@CaF_2 can be systematically intensified by increasing the core Yb doping ratio, resulting in a 9-fold increase in UV-emission compared to the known optimal ß-$NaYF_4$:Yb(30%),Tm(0.5%)@β-$NaYF_4$.[37] However, despite these advantages of the CaF_2 shell system in terms of UCNP engineering, the design and application of CaF_2-coated UCNPs are far more underdeveloped compared to more established β/β core/shell UCNPs.[38−41]

We envisioned that engineering CaF_2 coated UCNPs *via* doping high Yb concentrations in the core may be applied to α-$NaYF_4$:Yb,Er@CaF_2's structure to augment red-emission for *in vivo* deep tissue PDT applications. Herein, we report a facile method for amplifying the red-emission of $NaYF_4$:Yb,Er@CaF_2 by inherently adjusting the core Yb ratio from 20% to 98%, resulting in 15 times the red-emission of β-$NaYF_4$:Yb(20%),Er(2%)@β-$NaYF_4$ and a highest reported absolute quantum yield value (*i.e.*, 3.2 ± 0.1%) of red-emissions from UCNPs. Furthermore, we conjugate the prodrug 5-ALA to the UCNPs by means of a covalent hydrazone linkage to avoid possible preleaking of the ALA and thereby increase its bioavailability. Subsequently, with 980 nm light excitation, the optimally red-emitting UCNPs can cause the PpIX to produce singlet oxygen and trigger tumor cell death, as seen through a deep tissue simulation up to 1.2 cm in thickness both *in vitro* and *in vivo*. At a biocompatible power density of 0.5 W/cm^2, our red-emitting

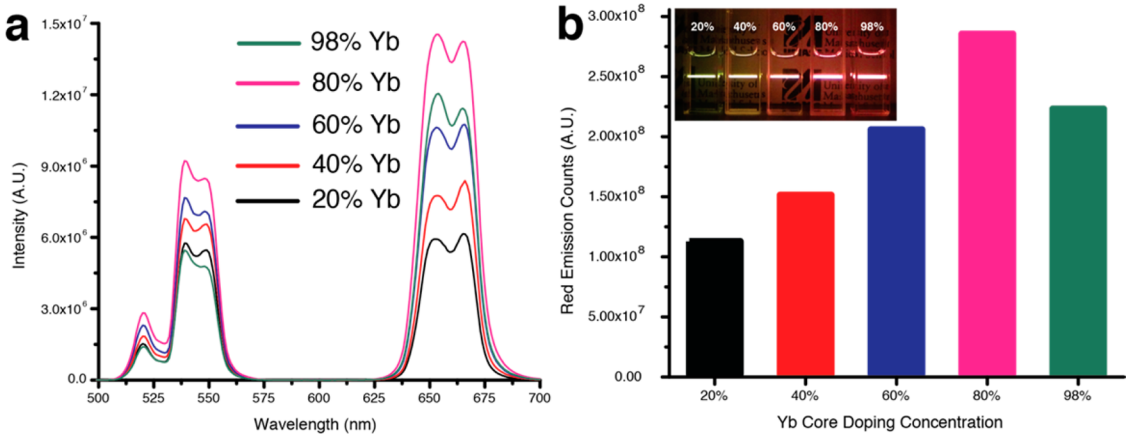

Figure 1. Emission spectra (a) under CW 980 nm, 1 W/cm^2 excitation of α-$NaYF_4$:Yb,Er@CaF_2 UCNPs with different Yb-levels. Integrated counts of red-emission (b) and photographs (inset) of α-$NaYF_4$:Yb,Er@CaF_2 UCNPs with different Yb-levels.

ALA−UCNP structure can still produce a significant cell killing effect through 1.2 cm of pork; when experimentally compared to the previously known optimal, however, this was not observed. Furthermore, *in vivo* PDT treatment shows our ALA−UCNP PDT system with low-power 980 nm irradiation outperforms clinically used red light irradiation in deep tumors, indicating a major step forward in improving the efficiency of deep-tissue PDT.

RESULTS AND DISCUSSION

Synthesis and Characterization of α-$NaYF_4$:Yb,Er(2%)@CaF_2 UCNPs. In our study, we synthesized a series of α-$NaYF_4$:Yb,Er(2%)@CaF_2 UCNPs with escalated Yb ratios (*i.e.*, 20%, 40%, 60%, 80%, 98%) similar to our established method.[37] These UCNPs have nearly the same average diameter of 26 nm (Supporting Information Figure S1a−e) and were further morphologically characterized by transmission electron microscopy (Supporting Information Figure S 1f−j) and X-ray diffraction (Supporting Information Figure S2), which show their uniform cubic core/shell structures.

To determine the optimal Yb ratio in this family of core/shell UCNPs, we characterized their red-emission outcome using spectrofluorimetry. Emission spectra under continuous wave (CW) 980 nm excitation of these UCNPs demonstrate that as the Yb core doping ratio increases from 20% to 80%, the red-emission increases systematically (Figure 1a). Integrated counts between 600 and 700 nm and corresponding photographs reveal that there is a 250% percent increase in red-emissions from α-$NaYF_4$:Yb(20%),Er(2%)@CaF_2 to α-$NaYF_4$:Yb(80%), Er(2%)@CaF_2 (Figure 1b and inset).

Furthermore, the red-emissions of α-$NaYF_4$:Yb(80%),Er(2%)@CaF_2 is 15 times as strong as that of β-$NaYF_4$:Yb(20%),Er(2%)@β-$NaYF_4$ (structurally sound as characterized in Supporting Information Figure S3), the supposed optimal red-emitting UCNP structure (Supporting Information Figure S4). The absolute quantum yield of $NaYF_4$:Yb(80%),Er(2%)@CaF_2 is measured to be 3.2 ± 0.1% under 10 W/cm^2, which is, to the best of our knowledge, the highest reported value for red-emissions. In addition, the extinction coefficient of UCNPs can also increase 4 times by elevating the concentration of the sensitizer (Yb^{3+}) from 20% to 80%. However, the 98% Yb (α-$NaYbF_4$: Er(2%)@CaF_2) had slightly less red-emission than 80% Yb, confirming that 80% is the optimal Yb core concentration for the red-emissions.

The 80%Yb α-core and 80%Yb@CaF_2 particles under TEM imaging show a distinct size distribution difference in Supporting Information Figure S11, indicating that they indeed form a core/shell structure as expected. In addition, the power-dependent curve of red-emission from α-$NaYF_4$:Yb(80%),Er(2%)@CaF_2 (Supporting Information Figure S5) indicates the luminescence is a two-photon upconverting process. In the Yb/Er upconversion process, Er^{3+} is quickly brought to the $^4S_{3/2}$ state by Yb's two-photon energy transfer. It is hypothesized that high Yb^{3+} concentration causes a back-energy-transfer from the $^4S_{3/2}$ state of Er^{3+} to the prevalent Yb. Delayed energy transfers from the excited Yb will bring the Er^{3+} to the $^4F_{9/2}$ state by multiphoton upconversion, leading to the enhanced red emission. This enhanced red emission occurs at 80% Yb instead of 98% because red-emission is a two-photon process, and thus is saturated before the maximum Yb concentrations. This early saturation was similarly observed with the blue and NIR emission of α-$NaYF_4$:Yb,Tm@CaF_2.[37]

Synthesis and Characterization of ALA-α-$NaYF_4$:Yb(80%),Er(2%)@CaF_2 UCNPs. We then functionalized α-$NaYF_4$:Yb(80%),Er(2%)@CaF_2 UCNPs for the aqueous phase and conjugated ALA to them with a pH-sensitive hydrazone linkage *via* the method represented in Supporting Information Figure S6. Thus, in this design, after such UCNPs enter the cell, conjugated ALA would be released by the low pH of the endosome,[42] and subsequently diffuse to the mitochondria and cause the

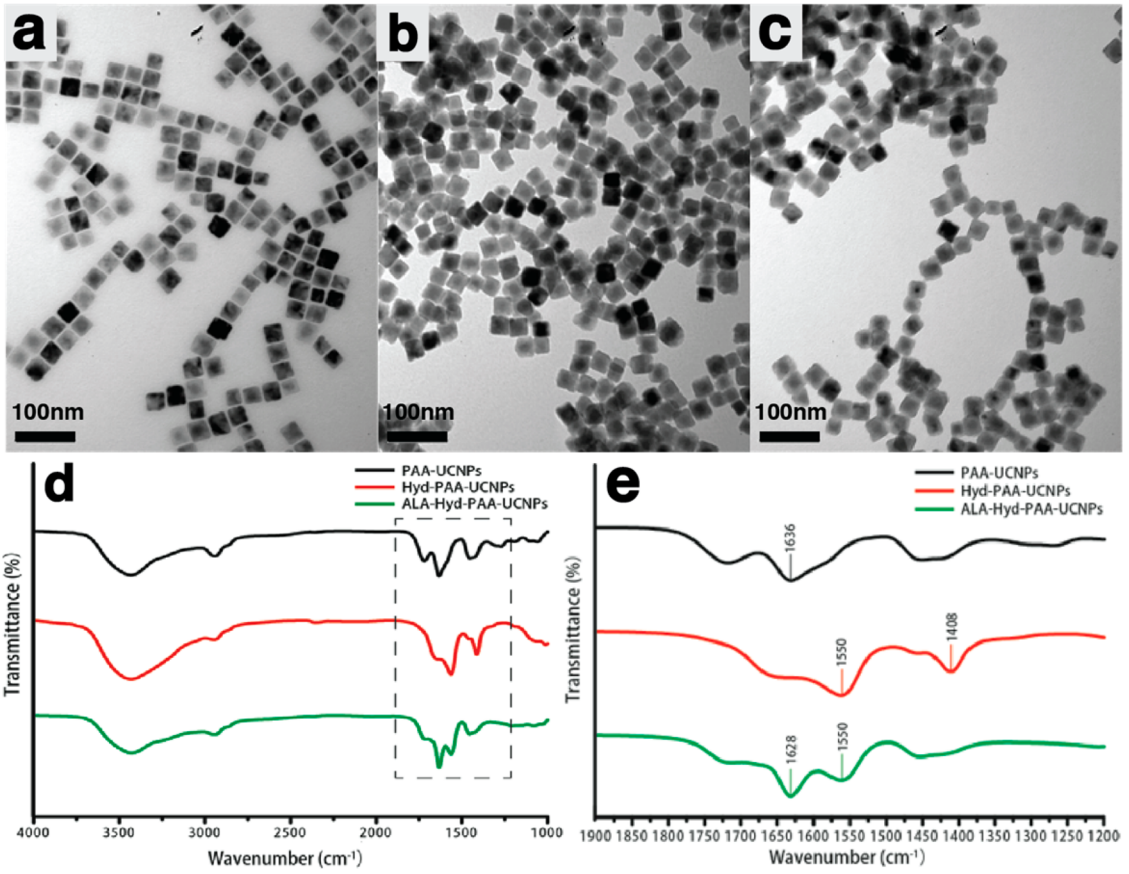

Figure 2. Characterization of hydrophilic UCNPs: TEM images of PAA−UCNPs (a), Hyd−UCNPs (b), and ALA−UCNPs (c). Full FTIR spectra (d) and partial detailed spectra (e) of PAA−UCNPs, Hyd−UCNPs, and ALA−UCNPs.

overproduction of PpIX. The afforded ALA-conjugated UCNPs were also characterized morphologically. TEM images illustrate their monodispersity (Figure 2a−c) and dynamic light scattering further determines the hydrodynamic size of ALA−UCNPs is about 62 nm (Supporting Information Figure S7).

FTIR spectral analysis was employed to confirm the conjugation of ALA to the UCNPs *via* a hydrazone linkage (Figure 2d,e). On the spectrum for poly(acrylic acid)-functionalized UCNPs (PAA−UCNPs), the peak at 1636 cm^{-1} is attributed to the resonance of the carboxyl groups. However, this peak disappears after its amidation with hydrazine, as two new peaks at 1550 and 1408 cm^{-1} arise. These are attributed to the N−H bending and stretching vibrations of NH_3^+ respectively. Finally, when the hydrazone linkage to ALA is constructed, the peak at 1628 cm^{-1} represents the —N═C— bond between the hydrazide-functionalized UCNPs (Hyd−UCNPs) and the ALA and the retention of the peak at 1550 cm^{-1} indicates the full acid-sensitive covalent linkage was successfully constructed between the ALA and the UCNPs.[42] High performance liquid chromatography was used to analyze the supernatants from ALA conjugation and revealed a ~40 μmol/mg loading capacity for ALA onto the Hyd−UCNPs.

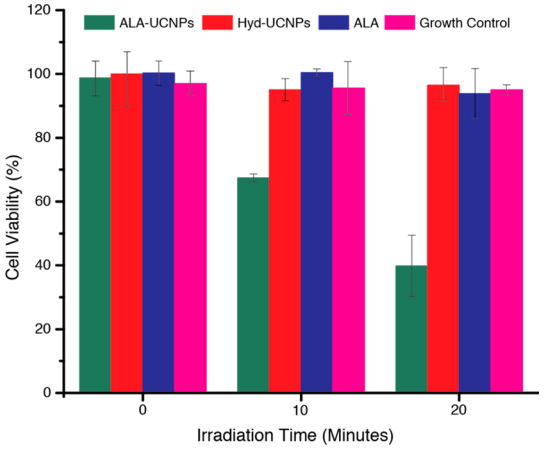

Figure 3. HeLa cell viability exposed to ALA−UCNPs (100 μg/mL), Hyd−UCNPs (100 μg/mL), free ALA (100 μg/mL), and nothing (growth control) and irradiated with CW 980 nm light at 0.5 W/cm^2 power density.

***In Vitro* Photodynamic Therapy Treatment.** To examine the PDT efficacy of ALA-conjugated UCNPs (80% Yb), we first conducted an MTT cell proliferation assay in which HeLa cells were exposed to ALA−UCNPs and various controls (all 100 μg/mL) for 4 h followed by irradiation of CW 980 nm light at 0.5 W/cm^2. It is important to note that 0.5 W/cm^2 is well below the

American National Standard for Safe Use of Lasers minimum permissible exposure for 980 nm CW laser of 0.73W/cm^2.[43] Cell viability data (Figure 3) indicates a time-dependent curve for cells exposed to ALA−UCNPs, resulting in almost 70% cell killing after 20 min, while the presence of Hyd−UCNPs, ALA without red light, and just NIR irradiation had minimal cytotoxicity.

Then, we sought to evaluate the impact of our red-emitting particles on ALA-induced photodynamic therapy. In this regard, we prepared β-$NaYF_4$:Yb(20%), Er(2%)@β-$NaYF_4$ ALA−UCNPs, the previously considered optimally red-emitting particle, with an similar ALA loading capacity (*i.e.*, ∼40 μmol/mg), and irradiated cells exposed to these nanoparticles at a biocompatible low power density of 0.5 W/cm^2. Figure 4 attests to the necessity of increasing the Yb ratio from 20% to 80% for phototherapeutic effect: while β-$NaYF_4$:Yb(20%),Er(2%)@β-$NaYF_4$ ALA−UCNPs have insignificant cell killing, α-$NaYF_4$:Yb(80%),Er(2%)@CaF_2 ALA−UCNPs have a more than 60% cell death after 20 min. It might be expected based on PpIX's absorbance spectrum (Supporting Information Figure S12) that the green emission of the β/β core/shell UCNPs activates PpIX leading to a therapeutic effect. However, after both β-$NaYF_4$:Yb(20%),Er(2%)@β-$NaYF_4$ and α-$NaYF_4$:Yb(80%),Er(2%)@CaF_2 were conjugated to ALA and transferred into the aqueous phase, Supporting Information Figure S13a illustrates that ∼95% of the green emission is quenched from the original emissions in hexane. This explains why the β/β core/shell ALA−UCNPs failed to induce cell death and confirms that the overlap between the red emission of the CaF_2-coated UCNPs and the red absorbance of PpIX (Supporting Information Figure S13b) is the main contributor to this PDT efficiency.

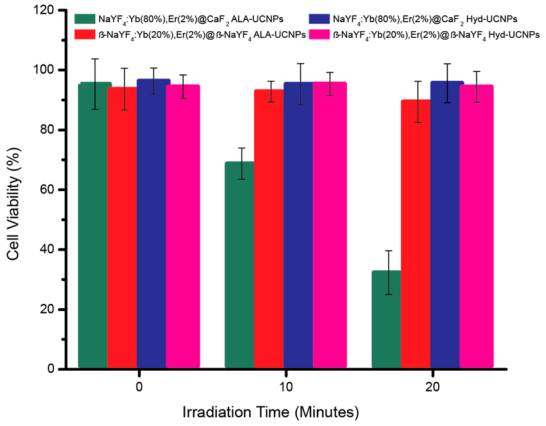

Figure 4. HeLa cell viability exposed to α-$NaYF_4$:Yb(80%), Er(2%)@CaF_2 and β-$NaYF_4$:Yb(20%),Er(2%)@β-$NaYF_4$ ALA−UCNPs (100 μg/mL) and α-$NaYF_4$:Yb(80%),Er(2%)@CaF_2 and β-$NaYF_4$:Yb(20%),Er(2%)@β-$NaYF_4$ Hyd−UCNPs (100 μg/mL) and irradiated with CW 980 nm light at 0.5 W/cm^2 power density.

Singlet Oxygen Generation Detection *in Vitro*:. To investigate the mechanism of the results from the above-mentioned experiments, we validated the production of PpIX and concomitant generation of singlet oxygen species caused by exposure to ALA−UCNPs. We stained cells with 2′,7′-dichlorofluorescein diacetate (DCFDA), a standard fluorescent indicator for singlet oxygen generation, and imaged using fluorescence microscopy (Figure 5). DCFDA diffuses into the cell and is acetylated into a nonfluorescent compound by cellular esterases. Reactive oxygen species (ROS) oxidizes it into 2′,7′-dichlorofluorescin (DCF), which has bright green fluorescence.[44] In our study, we found that cells exposed to ALA−UCNPs show intensifying DCFDA fluorescence over irradiation time, clearly indicating the production of PpIX and then singlet oxygen (Figure 5a−c). In addition, brightfield imaging overlaid with the UCNP emission (Supporting Information Figure S10) shows that the UCNPs are indeed in the cytoplasm, indicating they were instrumental in activating the PpIX.

This data was later corroborated with a quantification of the singlet oxygen production by measuring the fluorescence intensity of the DCFDA using 96-well

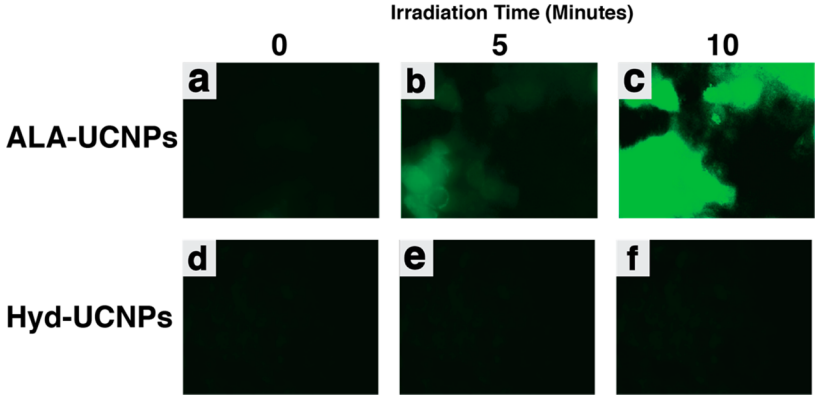

Figure 5. Singlet oxygen production detected by fluorescence of DCFDA in HeLa cells exposed to 100 μg/mL of ALA−UCNPs and irradiated with 0 (a), 5 (b), and 10 min (c) of CW 980 nm light. Singlet oxygen production detected by fluorescence of DCFDA in HeLa cells exposed to 100 μg/mL of Hyd−UCNPs and irradiated with 0 (d), 5 (e), and 10 min (f) of CW 980 nm light.

microtiter plate reader (Figure 6). Both DCFDA fluorescence imaging and microtiter plate measurement suggest effective prodrug delivery and subsequent PpIX activation by our red-emitting UCNPs.

***In Vitro* Deep-Tumor PDT Treatment.** Once we had established the optimal red-emission and PDT effect of 80% Yb UCNPs, we sought to simulate PDT in deep-set tumor conditions *in vitro*. In this regard, pieces of pork tissue of varying thickness were placed between the NIR laser and HeLa cells exposed to UCNPs (Figure 7a) and analyzed for cell viability with an MTT assay (Supporting Information Figure S8). It is also worth noting that with the added distance between the meat and cells (*i.e.*, the height of the well and the media bathing the cells), the simulated depths were greater than the measured thickness of the pork. After 40 min of irradiation at 0.5 W/cm^2, all pork thicknesses had cell viabilities significant to the control (Hyd−UCNPs). While no pork (0 mm) resulted in less than 20% cell viability, 6 mm had less than 50% cell viability and 12 mm had ~70% cell viability. This establishes and validates the feasibility of using UCNPs as a NIR-to-red transducer for prodrug photodynamic therapy at a deep-tissue level (>1 cm).

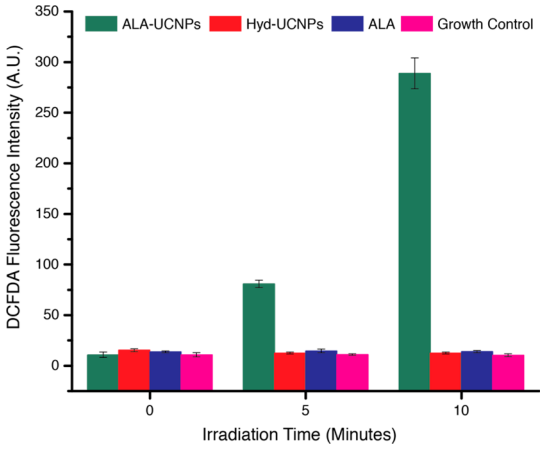

Figure 6. Singlet oxygen quantified by DCFDA fluorescence in HeLa cells exposed to 100 μg/mL of ALA UCNPs, Hyd−UCNPs, ALA, and nothing (growth control).

In addition, our novel red-emitting UCNP−PDT system was compared with the previously known optimal β/β core/shell red-emitting structure at a deep tissue level with a biocompatible low power density of 0.5 W/cm^2 for laser irradiation. Figure 7b demonstrates the dramatic improvement in phototherapeutic effect with our novel red-emitting UCNPs in ALA-PDT, with more than 30% cell death even with 1.2 cm of pork. In contrast, β/β core/shell ALA−UCNPs could not induce phototherapeutic effect, possibly because at such a low power density with superficial tissue, they cannot efficiently emit red light.

***In Vivo* Deep-Tumor PDT Treatment.** Finally, *in vivo* testing was conducted in subcutaneous tumors grown on Balb/c mice models to evaluate the effect of our PDT treatment. Here, we compared the tumor volume reduction effect of a red light laser ranging from ~635−685 nm (PpIX's activation region) and 980 nm light irradiation (UCNPs' activation wavelength) at a biocompatible 0.5 W/cm^2. After all tumors reached a normalized volume, they were separated into groups of five and injected with either ALA−UCNPs or saline (growth control and irradiation toxicity control groups). Then, they were irradiated on the first day with

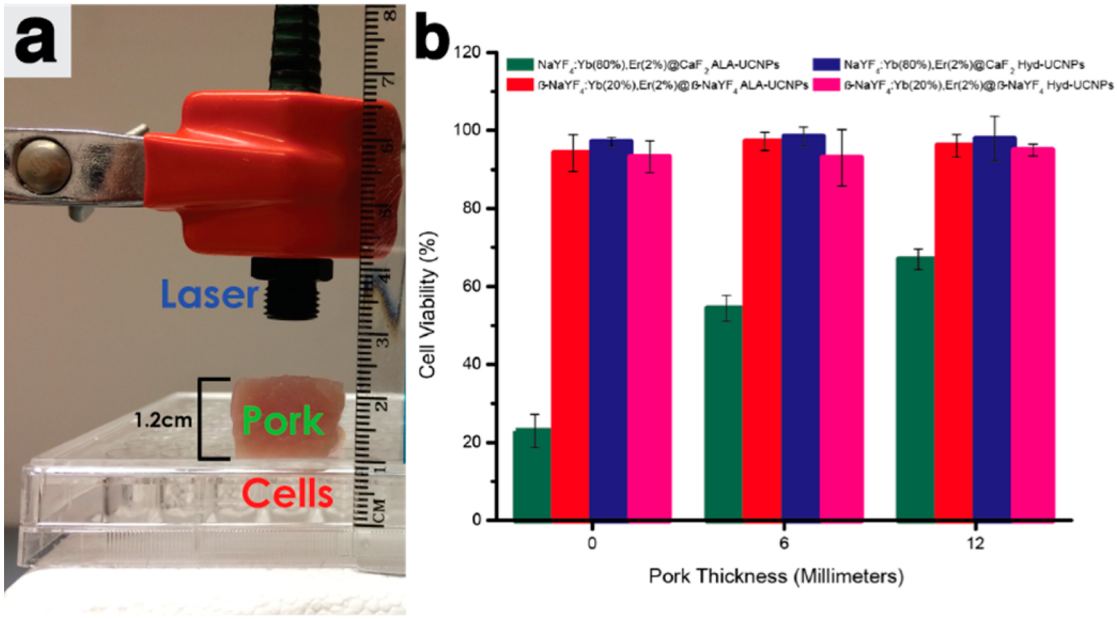

Figure 7. Photograph of the setup of simulated deep tumor conditions in an *in vitro* MTT assay (a). HeLa cell viability exposed to α-NaYF4:Yb(80%),Er(2%)@CaF_2 and β-NaYF4:Yb(20%),Er(2%)@β-NaYF4 ALA−UCNPs (100 μg/mL) and α-NaYF4:Yb(80%), Er(2%)@CaF2 and β-NaYF4:Yb(20%),Er(2%)@β-NaYF4 Hyd−UCNPs (100 μg/mL) and irradiated with CW 980 nm light at 0.5 W/cm^2 power density for 40 min with 0, 6, and 12 mm pork tissue on top of the cells (b).

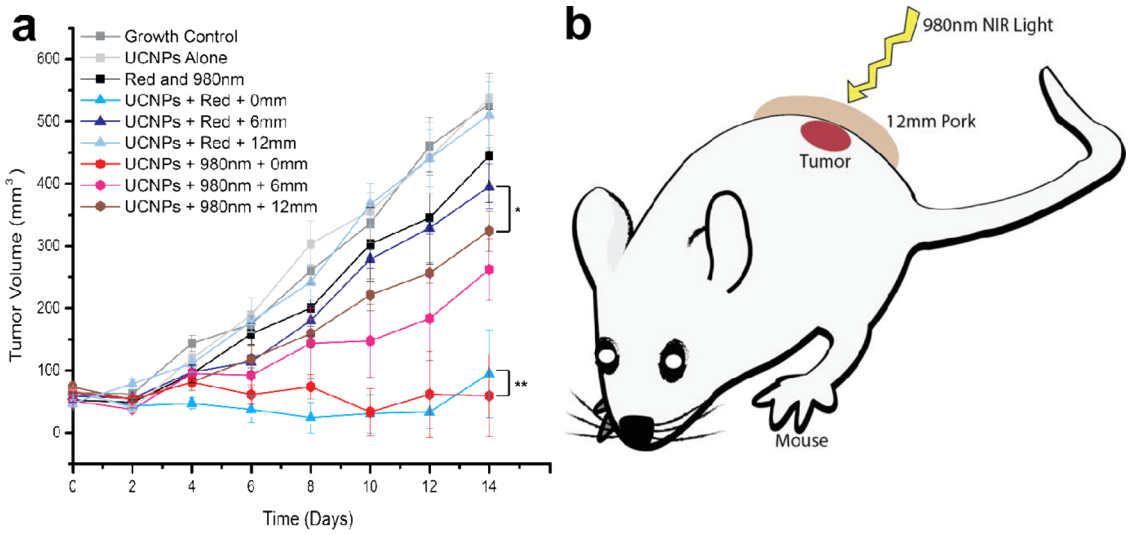

Figure 8. *In vivo* **volume of tumors exposed to various controls and ALA−UCNPs with red and near-infrared irradiation (0.5 W/cm^2) in simulated deep tumors. Legend: gray square, untreated tumors serving as growth controls; light gray square, tumors exposed to ALA−UCNPs and no irradiation; black square, tumors simultaneously exposed to red and NIR light both at 0.5 W/cm^2, but no ALA−UCNPs; blue triangle, tumors exposed to ALA−UCNPs and clinically used red light; navy blue triangle, tumors 6 mm deep exposed to ALA−UCNPs and clinically used red light; light blue triangle, tumors 12 mm deep exposed to ALA−UCNPs and clinically used red light; red hexagon, tumors exposed to ALA−UCNPs and deep-penetrating 980 nm light; magenta hexagon, tumors 6 mm deep exposed to ALA−UCNPs and deep-penetrating 980 nm light; brown hexagon, tumors 12 mm deep exposed to ALA−UCNPs and deep-penetrating 980 nm light. Statistical significance was determined from one-way *t* tests; significance (*) was based on $p < 0.05$ and $p > 0.05$ for not significant (**) pairs.**

their respective wavelength and tumor volume and body mass were measured over 14 days. As seen in Figure 8a, regarding the control groups, treatment with irradiation controls (red + 980 nm wavelengths together, each at 0.5 W/cm^2) and the UCNPs alone were nearly the same as the growth control, and body mass change data indicates there was no noticeable toxicity to the mice in this treatment (Supporting Information Figure S9). As for the experimental groups, without a deep tumor simulation, Figure 8a shows that there is no statistically significant difference between treatment with NIR (red hexagon curve) and red (blue triangle curve) light, indicating our UCNP−PDT system can compete with the clinical norm. However, the advantage of 980 nm light is evident when PDT treatment was conducted when inserting pork tissue between the laser and the mice tumors (Figure 8b) to simulate deep tumors. ALA−UCNPs with 980 nm light irradiation produced ~150 mm^3 tumor reduction even with 1.2 cm of pork tissue above the tumor, while there is no noticeable therapeutic effect with clinically used red light irradiation at that depth. Moreover, statistical significance tests reveal that even with thick 1.2 cm of superficial tissue, 980 nm light induces therapy that is significantly greater than the tumor reduction induced by red light with 6 mm of superficial tissue, showing that ALA−UCNP PDT treatment outcompetes clinically used treatment even in the shallow tumor setting. Our nanostructure's ability to induce significant phototherapeutic effect with such low power excitation yet thick superficial tissue represents a major improvement in the design of PDT materials.

CONCLUSIONS

In conclusion, we have developed high Yb doped UCNPs with a biocompatible CaF_2 shell with an optimal 15-fold increase in red-emissions compared to their hexagonal phased counterparts. The absolute quantum yield of α-$NaYF_4$:Yb(80%),Er(2%)@CaF_2 is measured to be 3.2 ± 0.1%, the highest reported value for red-emissions. Furthermore, we demonstrate conjugating ALA, a clinically used prodrug for the red-absorbing photosensitizer PpIX, to the UCNP surface *via* a hydrazone linkage, giving us exquisite control over their PDT effect in the cell. This photodynamic therapy system was tested for its therapeutic potential: it exhibited strong singlet oxygen generation and ~70% cell death after 20 min of NIR irradiation. Furthermore, significant cell death (~30%) was produced in simulated deep tumor conditions with as much as 12 mm of pork tissue and a biocompatible low power density of 0.5 W/cm^2 while ALA−UCNPs based on the known optimal red-emitting UCNP cannot. Finally, *in vivo* mice models of tumors when treated with these ALA−UCNPs demonstrated size reduction significant from the controls even under 12 mm of pork tissue (the greatest depth at which UCNP−PDT has been achieved), while clinically used red light could not. Thus, we envision that this study marks an

important step forward in biocompatible photodynamic therapy utilizing UCNPs to effectively access deep-set tumors at a low irradiation power density. It may also provide new opportunities for the a variety of applications using upconverting red radiation in photonics and biophotonics.

METHODS

Synthesis of α-$NaYF_4$:Yb,Er(2%)@CaF_2 PAA−UCNPs. The synthesis was modified from a previous work.[45] In brief, 10 mg of OA-UCNPs were dispersed in hexane and mixed with 0.20 g of nitrosonium tetrafluoroborate dissolved in DMF in a sealed vial overnight. Subsequently, UCNPs were precipitated with 2-propanol and centrifugally washed once in DMF. UCNPs dissolved in DMF were mixed with 10 mg of poly(acrylic acid) dissolved in DMF at 80 °C overnight. Finally, UCNPs were precipitated with 2-propanol and centrifugally washed twice in water.

Synthesis of α-$NaYF_4$:Yb,Er(2%)@CaF_2 Hyd−UCNPs. PAA−UCNPs dissolved in PBS at 1 mg/mL were exposed to 50 mg of EDC and 10 mg of sulfo-NHS for 4 h. Then, excess EDC and sulfo-NHS were washed off by centrifugation and carboxyl-activated PAA−UCNPs were redispersed in PBS. This dispersion was mixed with 5 mL of hydrazine monohydrate overnight and subsequently centrifugally washed several times in DI water.

Synthesis of α-$NaYF_4$:Yb,Er(2%)@CaF_2 ALA−UCNPs. Hyd−UCNPs were centrifugally washed into 10 mL of anhydrous methanol several times at 1 mg/mL. Then, 5 mL of ALA dissolved in anhydrous methanol at 10 mg/mL and a drop of dilute acetic acid for catalysis were mixed with the Hyd−UCNPs for 48 h. ALA−UCNPs were then centrifugally washed and dispersed in PBS at 5 mg/mL.

Absolute Quantum Yield Measurement. A cylindrical quartz cuvette containing the sample in hexane solution was placed in a calibrated integrating sphere in a Horiba Jobin Yvon Fluorolog-3 spectrometer. For the samples and for a hexane blank, emission spectra (600−730 nm) and spectra of scattered excitation light (970−990 nm) were recorded and corrected for the wavelength-dependent sensitivity of the apparatus at 10 W/cm^2. The absolute quantum yield (QY) of each sample was determined according to the equation, $QY = (I_{em,sample} - I_{em,blank})/(I_{ex,blank} - I_{ex,sample})$, where I_x is the integrated intensity of the emission (em) or scattering (ex) spectrum for the sample or blank.

Cell Viability Analysis by MTT Assay. A 96-well microtiter plate seeded with 1×10^4 HeLa cells/well was incubated overnight at 37 °C with 5% CO_2. Cells were subsequently exposed to 100 μg/mL of ALA−UCNPs, Hyd−UCNPs, ALA, or PBS for 4 h and then irradiated with CW 980 nm laser diode at 0.5 W/cm^2 for 0, 5, 10, or 20 min. After overnight incubation, cells were labeled with 12 mM solution of MTT in PBS for 4 h. Finally, the media was aspirated and replaced with 50 μL of DMSO and formazan absorbance was determined by a plate reader at 540 nm.

Singlet Oxygen Detection Cell Imaging. Glass-bottom confocal dishes seeded with 1×10^6 HeLa cells were incubated overnight at 37 °C with 5% CO_2. Cells were subsequently exposed to 100 μg/mL of ALA−UCNPs or Hyd−UCNPs for 4 h. Cells were washed three times with warmed Hank's Balanced Salt Solution (HBSS) and then stained with 25 μM DCFDA in HBSS for 45 min. With the use of a fluorescent microscope equipped with a CW 980 nm laser diode, DCFDA fluorescence was imaged with 495 nm excitation and 535 nm emission between 0, 5, and 10 min of irradiation using a 60× water-immersion objective lens.

Singlet Oxygen Detection Quantification. A 96-well microtiter plate seeded with 1×10^4 HeLa cells/well was incubated overnight at 37 °C with 5% CO_2. Cells were subsequently exposed to 100 μg/mL of ALA−UCNPs, Hyd−UCNPs, ALA, or PBS for 4 h and then stained with 25 μM DCFDA in HBSS for 45 min. After irradiation with CW 980 nm laser diode for 0, 5, or 10 min, DCFDA fluorescence was immediately determined with a plate reader with 495 nm excitation and 535 nm emissions.

Loading Efficiency Determination Using High Performance Liquid Chromatography (HPLC). After the ALA-conjugation process and centrifugation of fresh ALA−UCNPs, the methanol-based supernatant was saved and vacuum-dried, and leftover solutes (including unconjugated ALA) were redispersed in 2 mL of DI. This solution was evaluated with HPLC to determine the concentration of free ALA by a standard curve (264 nm detection wavelength) and backcalculation was used to determine the amount of ALA conjugated to the Hyd−UCNPs.

***In Vivo* Photodynamic Therapy Treatment.** Female Balb/c mice were purchased from Nanjing Peng Sheng Biological Technology Co. Ltd. and used under protocols approved by Soochow University Laboratory Animal Center. 4T1 cells (1×10^6) suspended in 40 μL of PBS were subcutaneously injected into the back of each female Balb/c mouse. After ∼6 days, the mice bearing 4T1 tumors were treated when the tumor volume reached ∼50 mm^3. The mice were divided into 9 groups (n = 5 per group) and intratumorally injected with ∼40 μL of saline, or ALA−UCNPs (20 mg/mL). An optical fiber-coupled 980 nm high power laser diode (Hi-Tech Optoelectronics Co., Ltd. Beijing, China) was used to irradiate tumors at a power density of ∼0.5 W/cm^2 for 40 min (1 min interval after each minute of irradiation). The tumor sizes were measured by a caliper every other day and calculated as the volume (tumor length) × (tumor width)^2/2. The body weight of mice was also measured with every tumor measurment and percent change was calculated by the formula (body weight today)/(body weight on day 0) × 100.

Conflict of Interest: The authors declare no competing financial interest.

Acknowledgment. G.H. was supported by a start-up fund through the University of Massachusetts Medical School, UMass CVIP Technology Development Award, and by National Institute of Health R01MH103133 and the Human Frontier Science Program. Work at the Molecular Foundry was supported by the Director, Office of Science, Office of Basic Energy Sciences, Division of Materials Sciences and Engineering, of the U.S. Department of Energy under Contract No. DE-AC02-05CH11231.

Supporting Information Available: Upconverting nanocrystal characterization, supplementary PDT treatment data, and synthesis methods. This material is available free of charge *via* the Internet at http://pubs.acs.org.

REFERENCES AND NOTES

1. Chatterjee, D. K.; Fong, L. S.; Zhang, Y. Nanoparticles in Photodynamic Therapy: An Emerging Paradigm. *Adv. Drug Delivery Rev.* **2008**, *60*, 1627–1637.
2. Dolmans, D. E. J. G. J.; Fukumura, D.; Jain, R. K. Photodynamic Therapy for Cancer. *Nat. Rev. Cancer* **2003**, *3*, 380–387.
3. Lovell, J. F.; Liu, T. W. B.; Chen, J.; Zheng, G. Activatable Photosensitizers for Imaging and Therapy. *Chem. Rev.* **2010**, *110*, 2839–2857.
4. Macdonald, I. J.; Dougherty, T. J. Basic Principles of Photodynamic Therapy. *J. Porphyrins Phthalocyanines* **2001**, *5*, 105–129.
5. Borgatti-Jeffreys, A.; Hooser, S. B.; Miller, M. A.; Lucroy, M. D. Phase I Clinical Trial of the Use of Zinc Phthalocyanine Tetrasulfonate as a Photosensitizer for Photodynamic Therapy in Dogs. *Am. J. Vet. Res.* **2007**, *68*, 399–404.
6. Kato, H.; Furukawa, K.; Sato, M.; Okunaka, T.; Kusunoki, Y.; Kawahara, M.; Fukuoka, M.; Miyazawa, T.; Yana, T.; Matsui, K.; *et al.* Phase II Clinical Study of Photodynamic Therapy Using Mono-L-Aspartyl Chlorin E6 and Diode Laser for Early Superficial Squamous Cell Carcinoma of the Lung. *Lung Cancer* **2003**, *42*, 103–111.

7. Collaud, S.; Juzeniene, A.; Moan, J.; Lange, N. On the Selectivity of 5-Aminolevulinic Acid-Induced Protoporphyrin Ix Formation. *Curr. Med. Chem.: Anti-Cancer Agents* **2004**, *4*, 301–316.
8. Dougherty, T. J.; Gomer, C. J.; Henderson, B. W.; Jori, G.; Kessel, D.; Korbelik, M.; Moan, J.; Peng, Q. Photodynamic Therapy. *J. Natl. Cancer Inst.* **1998**, *90*, 889–905.
9. Huang, Z. A Review of Progress in Clinical Photodynamic Therapy. *Technol. Cancer Res. Treat.* **2005**, *4*, 283.
10. Peng, Q.; Berg, K.; Moan, J.; Kongshaug, M.; Nesland, J. M. 5-Aminolevulinic Acid-Based Photodynamic Therapy: Principles and Experimental Research. *Photochem. Photobiol.* **1997**, *65*, 235–251.
11. Peng, Q.; Warloe, T.; Berg, K.; Moan, J.; Kongshaug, M.; Giercksky, K.-E.; Nesland, J. M. 5-Aminolevulinic Acid-Based Photodynamic Therapy. *Cancer* **1997**, *79*, 2282–2308.
12. Ericson, M. B.; Wennberg, A. M.; Larko, O. Review of Photodynamic Therapy in Actinic Keratosis and Basal Cell Carcinoma. *Ther. Clin. Risk Manag.* **2008**, *4*, 1–9.
13. Ntziachristos, V.; Bremer, C.; Weissleder, R. Fluorescence Imaging with near-Infrared Light: New Technological Advances That Enable *in Vivo* Molecular Imaging. *Eur. Radiol.* **2003**, *13*, 195–208.
14. Oar, M. A.; Serin, J. M.; Dichtel, W. R.; Fréchet, J. M. J.; Ohulchanskyy, T. Y.; Prasad, P. N. Photosensitization of Singlet Oxygen *via* Two-Photon-Excited Fluorescence Resonance Energy Transfer in a Water-Soluble Dendrimer. *Chem. Mater.* **2005**, *17*, 2267–2275.
15. Wang, S.; Gao, R.; Zhou, F.; Selke, M. Nanomaterials and Singlet Oxygen Photosensitizers: Potential Applications in Photodynamic Therapy. *J. Mater. Chem.* **2004**, *14*, 487–493.
16. Haase, M.; Schafer, H. Upconverting Nanoparticles. *Angew. Chem., Int. Ed.* **2011**, *50*, 5808–29.
17. Feng, W.; Han, C.; Li, F. Upconversion-Nanophosphor-Based Functional Nanocomposites. *Adv. Mater.* **2013**, *25*, 5287–5303.
18. Wang, F.; Banerjee, D.; Liu, Y.; Chen, X.; Liu, X. Upconversion Nanoparticles in Biological Labeling, Imaging, and Therapy. *Analyst* **2010**, *135*, 1839–1854.
19. Wang, F.; Liu, X. Recent Advances in the Chemistry of Lanthanide-Doped Upconversion Nanocrystals. *Chem. Soc. Rev.* **2009**, *38*, 976–989.
20. Wang, C.; Tao, H. Q.; Cheng, L.; Liu, Z. Near-Infrared Light Induced *in Vivo* Photodynamic Therapy of Cancer Based on Upconversion Nanoparticles. *Biomaterials* **2011**, *32*, 6145–6154.
21. Idris, N. M.; Gnanasammandhan, M. K.; Zhang, J.; Ho, P. C.; Mahendran, R.; Zhang, Y. *In Vivo* Photodynamic Therapy Using Upconversion Nanoparticles as Remote-Controlled Nanotransducers. *Nat. Med.* **2012**, *18*, 1580–U190.
22. Chatterjee, D. K.; Yong, Z. Upconverting Nanoparticles as Nanotransducers for Photodynamic Therapy in Cancer Cells. *Nanomedicine* **2008**, *3*, 73–82.
23. Liu, K.; Liu, X.; Zeng, Q.; Zhang, Y.; Tu, L.; Liu, T.; Kong, X.; Wang, Y.; Cao, F.; Lambrechts, S. A. G.; *et al.* Covalently Assembled Nir Nanoplatform for Simultaneous Fluorescence Imaging and Photodynamic Therapy of Cancer Cells. *ACS Nano* **2012**, *6*, 4054–4062.
24. Shan, J.; Budijono, S. J.; Hu, G.; Yao, N.; Kang, Y.; Ju, Y.; Prud'homme, R. K. Pegylated Composite Nanoparticles Containing Upconverting Phosphors and Meso-Tetraphenyl Porphine (Tpp) for Photodynamic Therapy. *Adv. Funct. Mater.* **2011**, *21*, 2488–2495.
25. Wang, C.; Tao, H.; Cheng, L.; Liu, Z. Near-Infrared Light Induced In vivo Photodynamic Therapy of Cancer Based on Upconversion Nanoparticles. *Biomaterials* **2011**, *32*, 6145–6154.
26. Qian, H. S.; Guo, H. C.; Ho, P. C.-L.; Mahendran, R.; Zhang, Y. Mesoporous-Silica-Coated Up-Conversion Fluorescent Nanoparticles for Photodynamic Therapy. *Small* **2009**, *5*, 2285–2290.
27. Wang, C.; Cheng, L.; Liu, Z. Drug Delivery with Upconversion Nanoparticles for Multi-Functional Targeted Cancer Cell Imaging and Therapy. *Biomaterials* **2011**, *32*, 1110–1120.
28. Tian, G.; Ren, W.; Yan, L.; Jian, S.; Gu, Z.; Zhou, L.; Jin, S.; Yin, W.; Li, S.; Zhao, Y. Red-Emitting Upconverting Nanoparticles for Photodynamic Therapy in Cancer Cells under near-Infrared Excitation. *Small* **2013**, *9*, 1929–1938.
29. Tian, G.; Gu, Z.; Zhou, L.; Yin, W.; Liu, X.; Yan, L.; Jin, S.; Ren, W.; Xing, G.; Li, S.; *et al.* Mn^{2+} Dopant-Controlled Synthesis of $NaYF_4$:Yb/Er Upconversion Nanoparticles for *in Vivo* Imaging and Drug Delivery. *Adv. Mater.* **2012**, *24*, 1226–1231.
30. Teng, X.; Zhu, Y.; Wei, W.; Wang, S.; Huang, J.; Naccache, R.; Hu, W.; Tok, A. I. Y.; Han, Y.; Zhang, Q.; Fan, Q.; Huang, W.; Capobianco, J. A.; Huang, L. Lanthanide-Doped NaxScF3+X Nanocrystals: Crystal Structure Evolution and Multicolor Tuning. *J. Am. Chem. Soc.* **2012**, *134*, 8340–8343.
31. Ding, Y.; Teng, X.; Zhu, H.; Wang, L.; Pei, W.; Zhu, J.-J.; Huang, L.; Huang, W. Orthorhombic KSc2F7:Yb/Er Nanorods: Controlled Synthesis and Strong Red Upconversion Emission. *Nanoscale* **2013**, *5*, 11928–11932.
32. Boyer, J.-C.; van Veggel, F. C. J. M. Absolute Quantum Yield Measurements of Colloidal $NaYF_4$: Er^{3+}, Yb^{3+} Upconverting Nanoparticles. *Nanoscale* **2010**, *2*, 1417–1419.
33. Krämer, K. W.; Biner, D.; Frei, G.; Güdel, H. U.; Hehlen, M. P.; Lüthi, S. R. Hexagonal Sodium Yttrium Fluoride Based Green and Blue Emitting Upconversion Phosphors. *Chem. Mater.* **2004**, *16*, 1244–1251.
34. Wang, Y.-F.; Sun, L.-D.; Xiao, J.-W.; Feng, W.; Zhou, J.-C.; Shen, J.; Yan, C.-H. Rare-Earth Nanoparticles with Enhanced Upconversion Emission and Suppressed Rare-Earth-Ion Leakage. *Chem.—Eur. J.* **2012**, *18*, 5558–5564.
35. Chen, G.; Shen, J.; Ohulchanskyy, T. Y.; Patel, N. J.; Kutikov, A.; Li, Z.; Song, J.; Pandey, R. K.; Ågren, H.; Prasad, P. N.; *et al.* (α-$NaYbF_4$:Tm^{3+})/CaF_2 Core/Shell Nanoparticles with Efficient near-Infrared to near-Infrared Upconversion for High-Contrast Deep Tissue Bioimaging. *ACS Nano* **2012**, *6*, 8280–8287.
36. Qiao, X.-F.; Zhou, J.-C.; Xiao, J.-W.; Wang, Y.-F.; Sun, L.-D.; Yan, C.-H. Triple-Functional Core-Shell Structured Upconversion Luminescent Nanoparticles Covalently Grafted with Photosensitizer for Luminescent, Magnetic Resonance Imaging and Photodynamic Therapy *in Vitro*. *Nanoscale* **2012**, *4*, 4611–4623.
37. Shen, J.; Chen, G.; Ohulchanskyy, T. Y.; Kesseli, S. J.; Buchholz, S.; Li, Z.; Prasad, P. N.; Han, G. Tunable Near-Infrared to Ultraviolet Upconversion Luminescence Enhancement in (α-$NaYF_4$:Yb,Tm)/CaF_2 Core/Shell Nanoparticles for in Situ Real-Time Recorded Biocompatible Photoactivation. *Small* **2013**, *9*, 3213–3217.
38. Wang, F.; Deng, R. R.; Wang, J.; Wang, Q. X.; Han, Y.; Zhu, H. M.; Chen, X. Y.; Liu, X. G. Tuning Upconversion through Energy Migration in Core-Shell Nanoparticles. *Nat. Mater.* **2011**, *10*, 968–973.
39. Wang, F.; Liu, X. G. Upconversion Multicolor Fine-Tuning: Visible to Near-Infrared Emission from Lanthanide-Doped $NaYF_4$ Nanoparticles. *J. Am. Chem. Soc.* **2008**, *130*, 5642–5643.
40. Wang, J.; Deng, R. R.; MacDonald, M. A.; Chen, B. L.; Yuan, J. K.; Wang, F.; Chi, D. Z.; Hor, T. S. A.; Zhang, P.; Liu, G. K.; *et al.* Enhancing Multiphoton Upconversion through Energy Clustering at Sublattice Level. *Nat. Mater.* **2014**, *13*, 157–162.
41. Wen, H. L.; Zhu, H.; Chen, X.; Hung, T. F.; Wang, B. L.; Zhu, G. Y.; Yu, S. F.; Wang, F. Upconverting near-Infrared Light through Energy Management in Core-Shell-Shell Nanoparticles. *Angew. Chem., Int. Ed.* **2013**, *52*, 13419–13423.
42. Dai, Y.; Yang, D.; Ma, P. A.; Kang, X.; Zhang, X.; Li, C.; Hou, Z.; Cheng, Z.; Lin, J. Doxorubicin Conjugated $NaYF_4$:Yb^{3+}/Tm^{3+} Nanoparticles for Therapy and Sensing of Drug Delivery by Luminescence Resonance Energy Transfer. *Biomaterials* **2012**, *33*, 8704–8713.
43. Chen, G.; Qiu, H.; Prasad, P. N.; Chen, X. Upconversion Nanoparticles: Design, Nanochemistry, and Applications in Theranostics. *Chem. Rev.* **2014**, *114*, 5161–214.
44. Bilski, P.; Belanger, A. G.; Chignell, C. F. Photosensitized Oxidation of 2′,7′-Dichlorofluorescin: Singlet Oxygen Does

Not Contribute to the Formation of Fluorescent Oxidation Product 2′,7′-Dichlorofluorescein. *Free Radical Biol. Med.* **2002**, *33*, 938–946.
45. Zhao, L.; Kutikov, A.; Shen, J.; Duan, C.; Song, J.; Han, G. Stem Cell Labeling Using Polyethylenimine Conjugated (α-$NaYbF_4$:Tm^{3+})/CaF_2 Upconversion Nanoparticles. *Theranostics* **2013**, *3*, 249–57.